Liquid Crystal Display Based Angle-of-Arrival Estimation of a Single Light Source

Andrej Harlakin, Adrian Krohn, and Peter A. Hoeher, *Fellow, IEEE*

***Abstract*—In this paper, a novel concept for visible light positioning is introduced, which employs a liquid crystal display as a dynamic optical filter in front of a photodetector. By electronically switching dedicated pixel areas in transparent or blocking mode, respectively, the angle of arrival is estimated. The measurement principle is supported by a mathematical model. Finally, an experimental setup is presented and measurement results are compared to the theoretical findings.**

***Index Terms*—Convolution, direction-of-arrival estimation, liquid crystal display, visible light positioning.**

I. Introduction

WHILE visible light communication (VLC) is a serious alternative to radio waves in short-range wireless communication, visible light positioning (VLP) has also been gaining interest in the research community [1]–[4]. Similar to VLC, VLP utilizes light in the visible range, which is predominantly generated by light emitting diodes (LED). In the likely event that these LEDs are also used for illumination, a particularly cost-effective and energy-efficient localization system can be implemented. In the experimental setup of this paper, focus will be on an LED light source (LS), but the measurement principle is valid for any point source.

Numerous optical localization algorithms exist that have their origins in radio frequency (RF) based positioning. One limitation regarding LED-based VLP, however, is that light emitting diodes produce non-coherent light, which prevents the use of phase information for localization. Well-known algorithms that are applicable in a non-coherent localization system can be classified into three types: proximity estimation, fingerprinting and triangulation [5].

Proximity estimation requires a large number of LED modules with known positions that are arranged in a dense grid. Furthermore, each module is programmed to transmit a unique identification code [6], [7]. Given the received code and the known position of the corresponding LED, the target device, e.g. photodetector (PD) with dedicated circuit, can estimate its own relative position. If a grid of LED light sources is already pre-installed, proximity estimation is a simple and efficient positioning technique. However, the drawback is the comparatively limited accuracy, which depends on the beamwidth of the LS as well as on the resolution of the lighting grid [4], [5].

Fingerprinting, also known as scene analysis, is a class of positioning algorithms that include a calibration phase in the estimation process. During this phase, extensive positioning measurements are conducted for every discrete anchor point inside an area of interest and stored in a database. Once the calibration is completed, the system conducts real-time positioning measurements and compares the results against the entries in the database. The entry that fits best with the real-time measurement is selected [8]. The key benefit of fingerprinting is the short run time after calibration. The drawback, however, is the performance in time-varying scenarios. In this case, an adaptive database is required, which is very time-consuming [4], [5].

Finally, triangulation is the umbrella term for a variety of localization algorithms, which utilize geometric properties of triangles [5]. Triangulation can be subdivided into two domains, lateration and angulation. Lateration estimates the position of a target device by measuring the distance to several anchor points, e.g. LED light sources. Algorithms that can be utilized for lateration are received signal strength (RSS), time-of-arrival (ToA) and time-difference-of-arrival (TDoA) estimation. While in RSS the known optical transmit power of several LS is used to calculate the position of a detection device [9], ToA and TDoA rely on signal runtime measurements. In ToA localization, the transmitter (Tx) units as well as the receiver (Rx) ones must be precisely synchronized, because the absolute signal runtime is measured [4]. TDoA, on the other hand, only requires a synchronization of the Tx, since only the difference of the transmit signal runtime is of interest [10]. To avoid ambiguity in RSS, ToA and TDoA, $N + 1$ signal sources, with N being the number of dimensions, are required. While lateration benefits from high localization accuracy, at the same time it requires a very high clock precision and very high sampling rates. This prevents the use of cheap of-the-shelf products [4].

The second domain of triangulation is direction-of-arrival estimation (DoA), also called angle-of-arrival (AoA) estimation, where the angle of arriving optical signals is measured. Compared to ToA and TDoA, no signal synchronization is required [4]. Several optical AoA estimation techniques have been published in recent times. One intuitive solution is to equip the target device with an array of PDs in a planar or circular arrangement. If the system is then illuminated by a LS, the

Manuscript received March 25, 2022; revised April 28, 2022; accepted April 30, 2022. Date of publication May 5, 2022; date of current version May 13, 2022. This work was supported by the Land Schleswig-Holstein within the Funding Programme Open Access Publikationsfonds. *(Corresponding author: Andrej Harlakin.)*

The authors are with the Department of Electrical and Information Engineering, Kiel University, 24143 Kiel, Germany (e-mail: anha@tf.uni-kiel.de; adkr@tf.uni-kiel.de; ph@tf.uni-kiel.de).

Digital Object Identifier 10.1109/JPHOT.2022.3172511

angle of arrival can be determined from the known distance and angle between the PDs and the difference in optical received power. In [11], for example, a system with three tilted PDs was developed. Due to this arrangement, each PD measures a different signal power, which enables two-dimensional positioning. By combining AoA with RSS measurements, three-dimensional (3D) positioning is possible with good accuracy. One challenge, however, is that the angle gain profile both of the Tx and Rx is required a priori.

A fundamentally different approach was proposed in [12]. There, the authors developed an AoA estimation system that consists of a quadrant PD located below a quadratic aperture. Because the cutout of the aperture is the size of the active PD area and is placed exactly over the detector, light impinging at an angle will result in different receive powers of the four quadrants of the PD. Given the known aperture height, and the dimension of the PD, the AoA can be calculated. It is shown that best results are obtained if the LS is directly above the Rx. The reason is the reduced signal power for an increased AoA. Furthermore, the technique is tailored to a single LS but could be extended to multiple LSs if orthogonal signals are used.

In this paper, we propose a novel concept in the domain of triangulation algorithms: we employ a liquid crystal display (LCD) as a dynamic receiver-side optical filter to estimate the AoA of a single LED LS.

To this day, LCD technology continues to attract the interest of researchers. In [13], for example, a 3D tensor display is developed, which consists of several stacked LCDs to support directional backlighting. While the goal of increased image fidelity is fundamentally different from our VLP approach, still in both cases the LCD is utilized to dynamically control the angle of light.

In our previous works [14]–[16], we proposed to use an LCD as a dynamic optical filter for ambient light and interference suppression in different VLC scenarios. For this purpose, the display is placed in front of a PD. By switching specific areas of the display opaque or transparent, undesired light sources can be suppressed while the signal of interest is passed to the PD. With this technique, an interference suppression of up to 35 dB was achieved. More recently, this principle has been extended to the field of optical underwater communication, particularly for high-rate communication between autonomous underwater vehicles [17].

In this paper, we propose to adapt the LCD interference suppression principle to AoA estimation in order to support visible light positioning. The configuration remains the same: the LCD acts as a dynamic receiver-side optical filter and is therefore placed in front of the PD. However, instead of suppressing unwanted light sources, the LCD is used to narrow the field of view (FoV) of the PD by switching a dedicated area transparent while leaving the remaining display opaque. That way, only signals from a specific direction are measured at the PD. To determine the AoA of a LS, the transparent area is then steered across the display and the light intensity is measured at the PD. Once the light intensity reaches its maximum, the transparent area lies exactly in the line of sight (LoS) between LED and PD. Then, from the known position of the transparent area the angle of the incident light can be estimated. For sufficiently slow time-varying environments, LCD-based AoA estimation can be combined with LCD-based interference suppression. This feature is not offered by existing VLP strategies. To the best of our knowledge, no technology has been developed so far that employs an LCD for AoA estimation in a visible light scenario. Accordingly, original contributions extending the state-of-the-art are as follows:

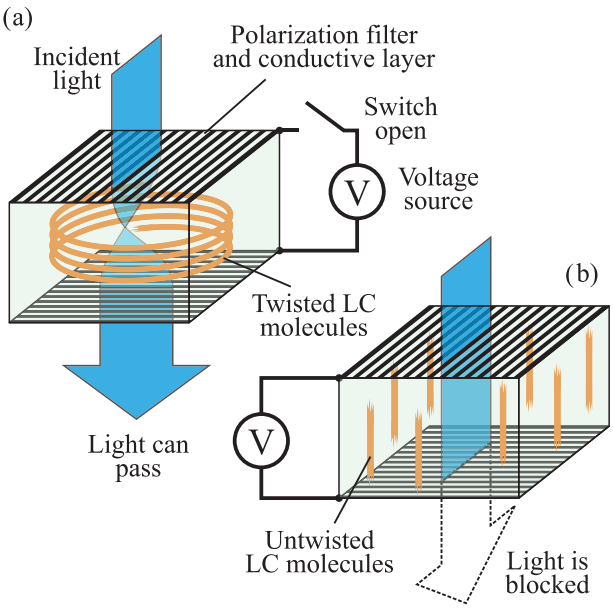

Fig. 1. Internal composition of an LC cell: (a) No voltage is applied and the LC molecules are in their regular twisted state. Incident light gets polarized by the first polarization filter. The LC molecules rotate the light's polarization, so it can pass the second polarization filter. (b) The LC molecules are untwisted by the applied electric field. The polarization of incident light is not changed and so it is blocked by the second polarization filter.

- A novel technique is introduced which determines the AoA of a single LS by utilizing a receiver-side LCD. The AoA can be estimated in two domains.
- A mathematical model of the LCD-based estimator is established. An analogon between convolution and LCD-based AoA estimation is pointed out.
- Performance results are evaluated and verified experimentally.

The remainder is organized as follows: In Section II, LCD technology is briefly described. The system model and an overview of the measurement principle are given in Section III. The experimental setup is introduced in Section IV. Performance results are presented in Section V. Finally, the conclusions are drawn in Section VI.

II. LCD Technology

An LCD consists of multiple liquid crystal (LC) cells, which are arranged in a grid. This structure can be seen as an LC array of individual pixels. These pixels can be switched continuously between a mode, where light can pass through the cell and another mode, where light is blocked. When used with a backlight, this arrangement is known as LCD. By adding color

filters, for example a red-green-blue (RGB) display is created. The principle of light blocking is realized by a compound of two orthogonal rotated polarization filters with LC molecules in between [18]. This structure and the basic process of interacting with light is depicted in Fig. 1. Incident light gets polarized by the first polarization filter and dependent on the state of the LC layer, the polarization is either rotated or left unaltered. If rotated, the light passes the second orthogonal polarization filter. If not, the light is blocked by the second filter and the pixel element appears dark. To change the state of the LC molecules, an electric field is needed. Therefore, transparent electrodes are used in order to apply a voltage. The electric field untwists the LC molecules, so they do not interfere with the light any more – the polarization is not changed. This type of display is known as *normally black*, as the display blocks all light without a voltage. By changing the orientation of one of the polarization layers, a *normally white* display is achieved.

The difference of the transmission factors in pass mode and in blocking mode should be as large as possible. In the pass mode, the transmission factor is affected by the polarization filters and by color filters. Furthermore, in pixel arrays, control circuits and address lanes for each pixel consumes a significant amount of space. For an off-the-shelf LC cell, transmission factors around 0.3 are reported in our previous works [14], [15]. In the blocking mode, we measured transmission factors as low as about 0.002. As this principle works best in the visible light range, an additional infrared-blocking filter can be added, dependent of the desired application.

The bare LC array without backlight can be used as an adaptive aperture to cast electronically-steerable shapes of shadows on a PD. When the dimensions of all system components are known, a receiver can estimate the AoA of a LS with the help of the LC array and the measured photocurrent.

III. System Model

A major limitation of LEDs is that the light emitted by diodes is non-coherent. Consequently, no phase information is available, which, for example, plays a key role in RF-based localization. On the receiver side, the same limitation persists. Typically, a PD is employed, which transforms light intensity into an electric current. No phase information can be extracted. Therefore, in this paper we propose a localization technique, which does not require the signal phase.

The idea is to place an LCD in front of the PD and employ the display as a receiver-side beam-steering device. To this end, a specific area of the LCD is switched transparent while the remaining pixels are kept in blocking mode. Because the LCD is a dynamic optical filter, the transparent area can be moved to every point on the display, i.e., also the beam of the PD can be steered to different directions. If, on top of that, measurements of the light intensity are carried out by the PD, direction information can be linked with intensity information.

This section explains in detail how the AoA information can be obtained from this setup. The first part describes the geometric scenario of the LCD-based AoA estimation setup. Besides the description of important AoA properties, special attention is paid to trade-offs that result from the geometrical model. The second part describes in detail the procedure which is applied to estimate the AoA of a LS. In the third part, the mathematical relationships are studied, which are required to prove assumptions from the previous parts and to interpret the measurement results in Section V. Finally, in the fourth part, results from the third part are supported by a calculation of the received optical power.

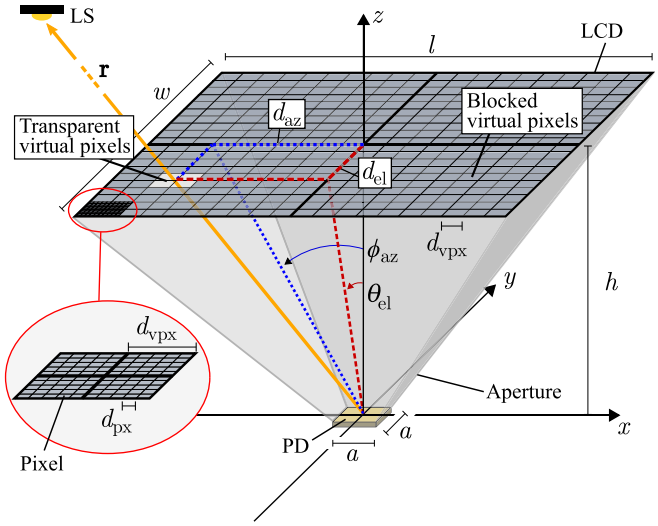

Fig. 2. Three dimensional geometrical model of LCD-based angle-of-arrival estimation.

A. Geometric Scenario

The AoA estimation system proposed in this paper consists of an LCD, a large-area PD, and an aperture that accommodates the LCD and the PD at a fixed position and distance. Fig. 2 depicts a 3D visualization of the arrangement. The PD has a square photosensitive area $A_{\mathrm{PD}} = a^2$ and its center is located at the origin of the xy-plane. Above it, at a distance h in z-direction, the LCD is mounted on the light impermeable aperture. Similarly to the PD, the center of the LCD is located at the origin of the xy-plane. The LCD has an active area $A_{\mathrm{LCD}} = l \cdot w$, with l being the length and w being the width of the display. A_{LCD} contains n_x pixels in x-direction and n_y pixels in y-direction, yielding a resolution of $n_x \times n_y$. The resulting edge length d_{px} of one quadratic pixel is given by

$$d_{\mathrm{px}} = \frac{l}{n_x} = \frac{w}{n_y}. \tag{1}$$

Nowadays, commercially available LCDs feature very high resolutions. In case the maximum resolution is not required for the LCD-based AoA estimation proposed in this paper, multiple pixels can be combined into larger 'virtual' pixels, i.e. areas in which all included pixels are controlled uniformly. The resulting edge length of the virtual pixels d_{vpx} depends on the chosen resolution $\kappa \in \mathbb{N}$, i.e. the number of pixels combined into one virtual pixel and can be calculated as $d_{\mathrm{vpx}} = \kappa \cdot d_{\mathrm{px}}$. Since the pixel edge length is increased by κ, the result is an artificial reduction of the LCD resolution to $\frac{n_x}{\kappa} \times \frac{n_y}{\kappa}$. Although

a reduction of the resolution might seem exclusively detrimental, this modification also offers a significant advantage in hardware implementation of the AoA estimator. A detailed explanation will be given in Section IV.

The FoV is an important property of AoA estimation systems that describes the angular range in which the AoA of a target device can be determined. In the proposed AoA estimation system, the FoV depends on the dimensions l and w of the LCD, the PD edge length a, and the distance h between LCD and PD. Since $l \neq w$ holds for most LCDs, both the FoV in azimuth $\mathrm{FoV}_{\mathrm{az}}$ as well as the FoV in elevation $\mathrm{FoV}_{\mathrm{el}}$ need to be specified:

$$\mathrm{FoV}_{\mathrm{az}} = 2 \cdot \arctan\left(\frac{l-a}{2h}\right) \tag{2}$$

$$\mathrm{FoV}_{\mathrm{el}} = 2 \cdot \arctan\left(\frac{w-a}{2h}\right). \tag{3}$$

Analyzing (2) and (3), one finds that the FoV is inversely proportional to the distance h between LCD and PD, i.e. an increase of h reduces the FoV.

Now assume that a single LS is located within the FoV of the LCD-based AoA estimator, cf. Fig. 2. Thus, a vector $\mathbf{r}$ can be defined which describes the LoS path between the LS and the PD. In this context, $h \ll \|\mathbf{r}\|_2$ applies, i.e. a far-field scenario is assumed. $\|\mathbf{r}\|_2$ denotes the Euclidean norm of $\mathbf{r}$ and describes its length. Initially, the LoS path is obstructed by the LCD. As known from Section II, the attenuation of the display in the opaque state is very high. Therefore, in order to establish a LoS connection, a pixel area A_{tran} is switched transparent and moved pixel-wise on the screen until the center of A_{tran} is intersected by $\mathbf{r}$. Once the transparent area lies directly in the LoS path, the PD measures the maximum light intensity. To determine the optimal size of A_{tran}, which is critical to the AoA estimation performance, the far-field assumption is considered. In other words it is assumed that the light emitted by the LS arrives as a planar wavefront at the LCD. Generally, three possibilities are applicable regarding the size of A_{tran}. First, A_{tran} can be larger than the photosensitive area of the PD, i.e. $A_{\mathrm{tran}} > A_{\mathrm{PD}}$. This, however, leads to ambiguous results because of the possibility that despite a position change of A_{tran}, still the full photosensitive area A_{PD} is illuminated. Thus, multiple angles can yield identical intensity measurement results. The second possibility is given by $A_{\mathrm{tran}} < A_{\mathrm{PD}}$. However, besides the fact that a reduction of the size of A_{tran} would also reduce the received power, the smaller area A_{tran} would also cause ambiguous results. In this case, there is a possibility that besides a position change of the transparent area, A_{tran} still fully overlaps A_{PD}. Thus, again multiple angles can yield identical measurement results. Therefore,

$$A_{\mathrm{tran}} = A_{\mathrm{PD}} = a^2 \tag{4}$$

is the optimal solution. In Section III-C, a mathematical analogy is identified and analyzed which supports this statement. This analogy is in turn supported by calculations in Section III-D.

To calculate the number of transparent pixels N_{tran} which are required to obtain A_{tran} with an active area of a^2 it must be considered that the LCD consists of an integer number of pixels, i.e., $N_{\mathrm{tran}} \in \mathbb{N}$. Therefore, the required number of pixels has to be rounded to

$$N_{\mathrm{tran}} = n_{\mathrm{tran}}^2 = \left\lfloor \frac{a}{d_{\mathrm{px}}} \cdot \frac{a}{d_{\mathrm{px}}} \right\rfloor. \tag{5}$$

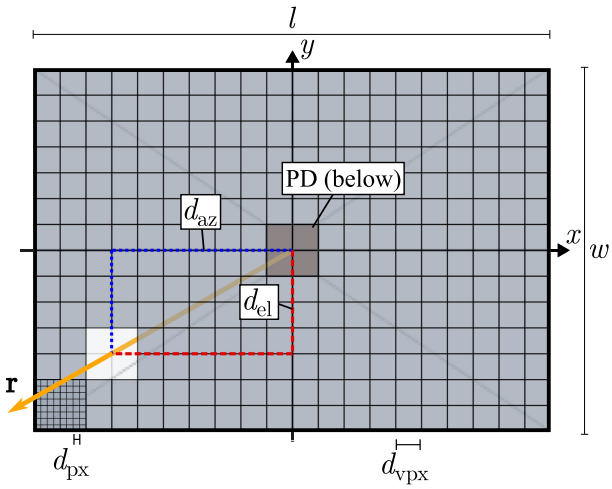

Fig. 3. Top view of LCD-based angle-of-arrival estimation.

The influence of a potential rounding error is investigated in Section IV.

To describe the AoA of the LS, two angles θ_{el} and ϕ_{az} are introduced. We define θ_{el} as the elevation angle, i.e. as the angle between the xz-plane and the projection of $\mathbf{r}$ onto the yz-plane. Furthermore, we define ϕ_{az} as the azimuth angle, i.e. as the angle between the yz-plane and the projection of $\mathbf{r}$ onto the xz-plane. Finally, we define d_{el} as the distance of the center of A_{tran} to the x-axis and d_{az} as the distance of the center of A_{tran} to the y-axis, cf. Fig. 3. Then, the angles of arrival ϕ_{az} and θ_{el} can be calculated as

$$\phi_{\mathrm{az}} = \arctan\left(\frac{d_{\mathrm{az}}}{h}\right) \tag{6}$$

$$\theta_{\mathrm{el}} = \arctan\left(\frac{d_{\mathrm{el}}}{h}\right). \tag{7}$$

At this point it should not go unmentioned that the LCD-based AoA estimator can measure angles only at discrete intervals. Again, the reason is that the LCD consists of an integer number of pixels. Therefore, d_{el} as well as d_{az} must be expressed as a multiple of a (virtual) pixel edge length d_{px}. As a result, for every (virtual) pixel the corresponding angles ϕ_{az} and θ_{el} can be calculated. Thus, a grid of discrete angles whose spacing depends on the LCD resolution is obtained.

Having defined the geometry of the setup as well as the angles ϕ_{az} and θ_{el}, the angular resolutions $\Delta\phi$ and $\Delta\theta$ of the LCD-based AoA estimator can be derived. We define the angular resolution as the angular difference between two (virtual) pixels. Since quadratic pixels are assumed, the angular resolution is equal for azimuth and elevation. Accordingly, we define $\xi = \Delta\phi = \Delta\theta$. The challenge, however, is that the pixels are arranged on a planar surface. Therefore, from the PD's perspective, the pixel edge length d_{px} of a quadratic pixel is effectively reduced with increasing AoA ϕ_{az} or θ_{el}. To derive a relationship that describes

the angular resolution as a function of the AoA, assume two adjacent pixels, i.e. the n-th and the $(n+1)$-th, with the n-th pixel at a distance $d_n = d_{\text{px}} \cdot \kappa \cdot n$ and the $(n+1)$-th pixel at a distance $d_{n+1} = d_{\text{px}} \cdot \kappa \cdot (n+1)$ from the origin, i.e. from the center of the LCD. Furthermore, assume two angles $\phi_{\text{az,n}}$ and $\phi_{\text{az,n+1}}$, $\theta_{\text{el,n+1}}$ and $\theta_{\text{el,n}}$, respectively, between the perpendicular of the PD, i.e. the z-axis, and the two pixels. Then, the angular difference $\xi = \phi_{\text{az,n+1}} - \phi_{\text{az,n}} = \theta_{\text{el,n+1}} - \theta_{\text{el,n}}$ can be described as

$$\xi = \arctan\left(\frac{(n+1)\, d_{\text{px}}\, \kappa}{h}\right) - \arctan\left(\frac{n\, d_{\text{px}}\, \kappa}{h}\right). \tag{8}$$

Finding a suitable addition theorem, the equation can be modified as follows:

$$\xi = \arctan\left(\frac{d_{\text{px}}\, h\, \kappa}{h^2 + n(n+1)\, d_{\text{px}}^2\, \kappa^2}\right). \tag{9}$$

To obtain an angular resolution that depends on the AoA, (6) and (7) can be transformed with $d_{\text{az}} = d_{\text{el}} = n \cdot d_{\text{px}} \cdot \kappa$. Inserting the equations in (9) yields

$$\begin{aligned}\xi(\phi_{\text{az}}) &= \arctan\left(\frac{d_{\text{px}}\, h\, \kappa}{h^2 + \tan^2(\phi_{\text{az}})\, h^2 + \tan(\phi_{\text{az}})\, h\, d_{\text{px}}\, \kappa}\right)\\ \xi(\theta_{\text{el}}) &= \arctan\left(\frac{d_{\text{px}}\, h\, \kappa}{h^2 + \tan^2(\theta_{\text{el}})\, h^2 + \tan(\theta_{\text{el}})\, h\, d_{\text{px}}\, \kappa}\right)\end{aligned} \tag{10}$$

with $\kappa = 1$ for hardware pixel sizes and $\kappa > 1$ for virtual pixel sizes. A considerable simplification of (10) results for the case where the LS is located in boresight in front of the LCD, i.e. $\phi_{\text{az}} = \theta_{\text{el}} = 0$:

$$\xi(0) = \arctan\left(\frac{d_{\text{px}}\, \kappa}{h}\right). \tag{11}$$

At the same time, this is the case where the LCD has the most coarse resolution. As the angle increases, the angular resolution becomes finer. Comparing (2), (3) with (11) one finds that the proposed AoA estimation setup creates a trade-off between the FoV and the angular resolution: to improve angular resolution, i.e. to reduce ξ, either the virtual pixel size $d_{\text{vpx}} = \kappa \cdot d_{\text{px}}$ has to be reduced or the height h has to be increased. In the latter case, however, the FoV is reduced. Depending on the application, a measurement system can therefore be developed that is either very accurate or covers a wide field of view. This trade-off will be further analyzed in Section IV.

B. Angle-of-Arrival Estimation

In this introductory paper, we restrict investigations to the AoA estimation of a single LS. Therefore, assume that one active LED is placed at an unknown position in the FoV of the AoA estimator.

Since the transparent square area A_{tran} can be moved to every grid point on the active area A_{LCD} of the LCD, the entire FoV of the system, which is limited by the aperture and its height h, can be scanned. In the absence of a-priori information, a meander-like search is suitable for this purpose, where the square area is moved line by line along the LCD axes. In the following, this strategy will be referred to as exhaustive search algorithm. If, moreover, a measurement of the incident light intensity is taken and stored during the scanning process after each reorientation of A_{tran}, one obtains light intensity information for every grid point. At some point during the scanning process the transparent area A_{tran} will lie in the LoS between the PD and the LS. For simplicity assume that exactly the center of A_{tran} is intersected by $\mathbf{r}$, i.e. the estimation is error-free, as shown in Fig. 2. In this case, the PD measures the maximum light intensity. Finally, in order to determine the angles of arrival ϕ_{az} and θ_{el} using (6) and (7), the distances d_{az} and d_{el} have to be derived. Fortunately, this step is straightforward because it is always known which pixels are switched transparent.

However, if the exhaustive search algorithm is chosen, one encounters a challenge in the use of hardware components. Nowadays, commercially available LCDs feature very high resolutions $n_x \times n_y$, but the frame rate $f_{\text{LCD}} = 1/T_{\text{LCD}}$, i.e. the rate at which liquid crystal panels update the image displayed on the screen, has improved only marginally. If the entire FoV is scanned by an exhaustive search, the runtime is

$$\frac{n_x n_y}{\kappa^2} \cdot T_{\text{LCD}}. \tag{12}$$

For high resolutions, an extremely high runtime can be expected. Numerical values are provided in Section IV-B. There are several approaches to this challenge. First of all, the exhaustive search can be combined with hill-climbing or comparable strategies, whose goal is to find the best-fitting solution and then terminate the search. Transferred to LCD-based AoA estimation, the algorithm will stop as soon as the maximum light intensity is found. That way, the expected runtime can be halved. Another approach is an artificial reduction of the resolution by increasing κ and creating virtual pixels. However, a significant reduction would be necessary for high-resolution displays to provide a practicable runtime. This would cause the system to suffer a substantial loss of accuracy.

An alternative to the meander-like search is what we call the bar algorithm. It searches the whole active LCD area with the help of transparent bars instead of a transparent square area A_{tran}, as depicted in Fig. 4. Obviously, for non-ambiguous measurement results, the width of the bars is as important as the size of A_{tran} in the exhaustive search algorithm. The optimal width is given as $d_{\text{vrt}} = d_{\text{hrz}} = a$, i.e., as the edge length of the photosensitive area of the PD. A mathematical analogy supporting this statement is provided in Section III-C. In the first run, a vertical bar of width d_{vrt} is generated to scan the LCD along the x-axis, i.e., in azimuth direction. In the second run, a horizontal bar of width d_{hrz} is generated to scan along the y-axis, i.e., in elevation direction. The bar algorithm reduces the maximum search runtime to

$$\frac{n_x + n_y}{\kappa} \cdot T_{\text{LCD}}. \tag{13}$$

The main reason is that in the argument the number of pixels in x-direction n_x and y-direction n_y now appears as an addition instead of a multiplication. Again, the expected runtime can be halved, if the algorithm is combined with hill-climbing or comparable strategies to stop iteration as soon as the maximum

light intensity is found. A further reduction can be achieved by generating virtual pixels, e.g. $\kappa = 10$. Again, numerical values for the algorithm runtime are provided in Section IV-B.

In the following, the procedure required to determine the AoA of the LS using the bar algorithm is described. In the initial step, the LCD generates a vertical transparent bar (cf. Fig. 4) of width d_{vrt} and places it in such a way that the center of the bar is located at $x = -\frac{l}{2}$. Then, the bar is moved in iterative steps along the discrete (virtual) pixel grid in x-direction until the center of the bar reaches the right edge, i.e., $x = \frac{l}{2}$. Subsequently, the horizontal transparent bar of width d_{hrz} is generated with its center at $y = -\frac{w}{2}$ and moved along the discrete (virtual) pixel grid in y-direction until the top edge, i.e. $y = \frac{w}{2}$, is reached. Evidently, the number of iterations required to reach a certain edge is equal to the number of (virtual) pixels in the respective direction.

After each iteration, the PD takes a light intensity measurement and the system stores the values in two measurement arrays, μ_{az} for x- (azimuth) direction and μ_{el} for y- (elevation) direction. Consequently, the number of entries in μ_{az} is equal to the number of (virtual) pixels in x-direction $\frac{n_x}{\kappa}$ and the number of entries in μ_{el} is equal to the number of (virtual) pixels in y-direction $\frac{n_y}{\kappa}$. We define the measurement arrays and their entries as

$$\mu_{\text{az}} = \left[m_{\text{az},1}, \ldots, m_{\text{az},p_{\text{max}}}, \ldots, m_{\text{az},P}\right] \tag{14}$$

$$\mu_{\text{el}} = \left[m_{\text{el},1}, \ldots, m_{\text{el},q_{\text{max}}}, \ldots, m_{\text{el},Q}\right]. \tag{15}$$

Furthermore, we define p and q as the indices of the measurement arrays with $P = \frac{n_x}{\kappa}$ and $Q = \frac{n_y}{\kappa}$. In the next step, the system searches for the maximum values of the light intensity $m_{\text{az},p_{\text{max}}}$ and $m_{\text{el},q_{\text{max}}}$ in both arrays. The maximum intensities are measured when the center of the respective transparent bar is intersected by $\mathbf{r}$, or in other words, when the transparent bar lies directly in the LoS between LED and PD. Storing the measured intensity values in an array offers a decisive advantage in this context: not only the maximum intensity value, but also its position within the array, i.e. its index p_{max}, q_{max}, can be determined. Thus, since the number of array entries is equal to the number of pixels, the system is able to determine w_{el} and l_{az}, which describe the distance the transparent bars travel from the starting point to the position where the maximum intensity was measured:

$$l_{\text{az}} = p_{\text{max}} \cdot \kappa \cdot d_{\text{px}} + \frac{d_{\text{vrt}}}{2} \tag{16}$$

$$w_{\text{el}} = q_{\text{max}} \cdot \kappa \cdot d_{\text{px}} + \frac{d_{\text{hrz}}}{2}. \tag{17}$$

The reason for the addition of half the bar widths d_{vrt}, d_{hrz} to the distances l_{az} and w_{el} can be attributed to the generation of the transparent bar: the position is determined by the bottom left pixel. For a correct angle measurement, however, the distance to the center of the transparent bar is required.

Finally, to calculate the angles of arrival ϕ_{az} and θ_{el} using (6) and (7), d_{az} and d_{el} can be derived as

$$d_{\text{az}} = -\frac{l}{2} + l_{\text{az}} \tag{18}$$

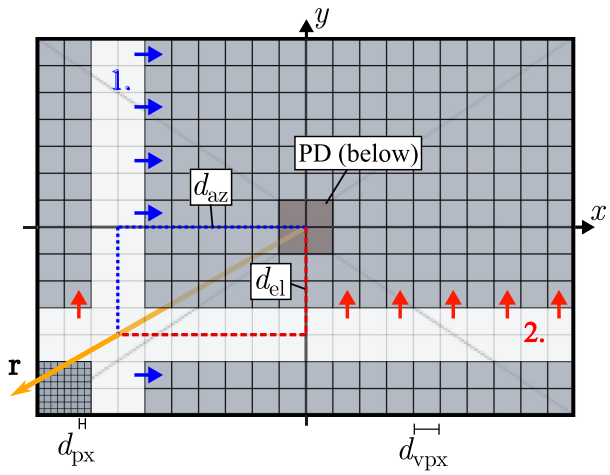

Fig. 4. Top view of LCD-based angle-of-arrival estimation with the bar algorithm.

$$d_{\text{el}} = -\frac{w}{2} + l_{\text{el}}. \tag{19}$$

Since the origin of the coordinate system is placed at the center of the LCD, half of the respective side length has to be subtracted.

C. Mathematical Analogy

To find a mathematical analogy describing the LCD-based AoA estimator, assume that a single LS is located at the origin of the xy-plane at a distance $\|\mathbf{r}\|_2$, i.e. exactly perpendicular to the PD. As specified in Section III-A, a far-field scenario $h \ll \|\mathbf{r}\|_2$ is supposed. Furthermore, assume an optimal LCD, which has a transmission factor of 1in pass mode and 0in blocking mode. Finally, assume that the LCD aperture has a reflection coefficient of 0, thus no light is reflected onto the PD.

In the initial state, the LCD is opaque. Then, a square transparent area $A_{\text{tran}} = A_{\text{PD}}$ (cf. Fig. 3) is generated with its center at $x = -\frac{l}{2}$, $y = 0$ and moved along the x-axis. As long as the transparent area A_{tran} does not overlap the square photosensitive area A_{PD} of the PD, no light intensity is measured. However, when A_{tran} reaches $x = -\frac{a}{2}$, both areas start to overlap and photons are detected. The maximum light intensity is reached when both areas completely overlap. As soon as A_{tran} is moved further along the x-axis, the light intensity is reduced again. Thus, it can be concluded that the measured light intensity is proportional to the overlapped area of the two squares. Interestingly, this principle exactly replicates the convolution operation. The measured light intensity at the position $x = x_0$ represents the overlap of the areas, i.e. the result of the convolution at $x = x_0$. More precisely, sliding a square transparent area A_{tran} over the square photosensitive area A_{PD} replicates a convolution of a rectangular function $f(x)$ with another rectangular function $g(x)$. The rectangular function of width X centered at $x = 0$ is commonly defined as

$$\text{rect}\left(\frac{x}{X}\right) = \begin{cases} 1, & \text{if } -\frac{X}{2} < x < \frac{X}{2} \\ \frac{1}{2}, & \text{if } x \in \{-\frac{X}{2}, \frac{X}{2}\} \\ 0, & \text{else.} \end{cases} \tag{20}$$

Since $A_{\text{tran}} = A_{\text{PD}}$ was previously specified, both rectangular functions have the same width X. The convolution of two functions $f(x)$ and $g(x)$ is defined as

$$(f * g)(x) := \int_{-\infty}^{\infty} f(\tau)\, g(x-\tau)\, d\tau. \tag{21}$$

Inserting both rectangular functions in (21) with $f(x)$, i.e. the photosensitive area of the PD, centered at $x = 0$, one obtains

$$\begin{aligned}(f * g)(x) &= \frac{1}{X} \int_{-\infty}^{\infty} \text{rect}\left(\frac{\tau}{X}\right) \text{rect}\left(\frac{x-\tau}{X}\right) d\tau \\ &= \text{tri}\left(\frac{x}{X}\right). \end{aligned} \tag{22}$$

As known from signal theory, the convolution yields a triangular function of width $2X$ centered at $x = 0$. Fig. 5 shows the result of a Matlab simulation in which two rectangular functions are convolved. For a good comparability with the measurement results in Section V, the x-axis is replaced by pixel indices, i.e. two rectangular functions of width $X_f = X_g = 210$ are convolved over a range of 2560 pixels. Furthermore, it is assumed that $f(x)$ is centered around the 1280th pixel. As can be seen in Fig. 5, the blue line depicts a triangular function with a width of $2X_f = 2X_g = 420$ pixels and its height normalized to 1.

Accordingly, the measurement result of the LCD-based AoA estimation setup will also yield a triangular function where the maximum of the triangular function represents the maximum light intensity which is measured when both rectangles completely overlap. This assertion will be verified in Section V, where measurement results are compared with analytical results.

Incidentally, the analogy between convolution and LCD-based AoA estimation also applies for the bar algorithm introduced in Section III-B. One key difference to the square transparent area is that for each position in x- and y-direction a measurement of the whole width respectively height of the LCD is taken. Still, the measured light intensity is proportional to the overlapped area. Therefore, in a scenario with only a single LS the results are the same. Again, a comparison to measurement results will be provided in Section V. The fact that the measurement signal represents a triangular function offers a decisive advantage. Since there is only one maximum, there are no ambiguities in the AoA estimation process. However, this is only the case if the two square areas A_{tran} and A_{PD} respectively the bar and A_{PD} have an absolutely equal width, i.e. the rectangular functions have an equal width X. Otherwise, the result of the convolution changes from a triangular function to an isosceles trapezoid as can be seen in Fig. 5. This applies both to the case when $g(x)$ is larger ($X_f < X_g$, yellow line) or smaller ($X_f > X_g$, orange line) than $f(x)$. In the first case, $g(x)$ has a width of 420 pixels, in the second case $g(x)$ has a width of 105 pixels.

The challenge in either case is that the measurement result contains sections where equal light intensities are measured. Because in the presented system the AoA is estimated by determining the maximum light intensity value, ambiguity is added and the imprecision of the technique is increased. This

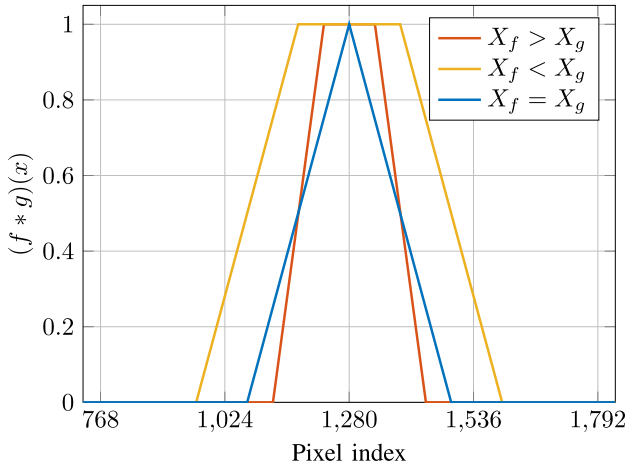

Fig. 5. Convolution of two rectangular functions $f(x)$ and $g(x)$ with varying widths X_f and X_g.

verifies the results about the optimal width of the transparent area determined in Section III-A.

At this point, it is important to mention that while it is straightforward to guarantee an equal width of $f(x)$ and $g(x)$ in a simulation, it is very challenging in a real LCD-based system. The reason is mentioned in Section III-A. An LCD consists of an integer number of pixels. Therefore, the required number of pixels to produce a transparent area (bar or square) of width X have to be rounded to an integer. Fortunately, using an LCD with a high resolution, the deviation is small. An investigation of a potential rounding error is provided in Section IV.

D. Radiometric Computation of the Received Power

In this section, we support the results reported in Section III-C by a radiometric computation of the received optical power at the PD of the LCD-based AoA estimator. We define P_{T} as the optical transmit power and m as the mode number of the LS, which is modeled as a generalized Lambertian source [4]. Let $r = \|\mathbf{r}\|_2$ denote the distance between Tx and Rx. Furthermore, we denote the LCD transmission factors in the pass mode and in the blocking mode as $g_{\text{LC},1} \in [0,1]$ and $g_{\text{LC},0} \in [0,1]$, respectively. To model the overlap of A_{tran} over A_{PD}, we define A_{cut} as the intersection of A_{tran} and the projected area of the PD along the LoS onto the LCD plane. Then, the optical receive power can be expressed as

$$\begin{aligned}P_{\text{R}} = P_{\text{T}} \cdot \frac{m+1}{2\pi} \cos^m(\vartheta) \\ \cdot \frac{1}{r^2} \left(A_{\text{cut}} \cdot g_{\text{LC},1} + (A_{\text{PD}} - A_{\text{cut}}) \cdot g_{\text{LC},0}\right) \cdot \cos(\vartheta) \end{aligned} \tag{23}$$

with

$$\vartheta = \arctan\left(\frac{\sqrt{d_{\text{az}}^2 + d_{\text{el}}^2}}{h}\right), \tag{24}$$

where ϑ is the angle between $\mathbf{r}$ and the z-axis. By shifting A_{tran} over A_{PD} and computing (23) for $A_{\text{cut}} \in [0, A_{\text{PD}}]$, first for linearly increasing and subsequently for linearly decreasing values, the result in Fig. 5 is validated. The maximum received optical

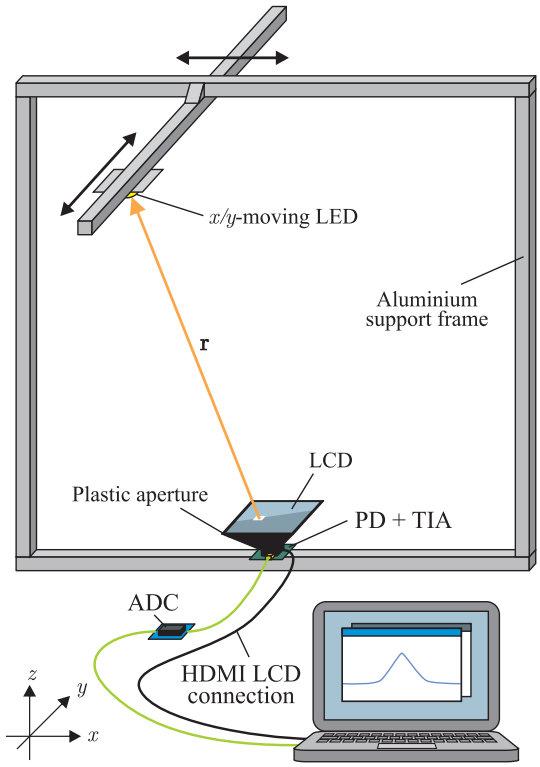

Fig. 6. Experimental setup of LCD-based AoA estimation.

power is given for $A_{\text{cut}} = A_{\text{PD}}$. The corresponding irradiance can be derived by dividing P_{R} by A_{PD}. In the following sections, we use the relative receive power, where the maximum receive power is normalized to one.

IV. Experimental Setup

This section is divided into three parts. The first part describes all hardware components used in the experimental setup and specifies the parameters. The second part determines the influence of different parameters on the AoA estimation system. Finally, the third part describes in detail the procedure of the LCD-based AoA estimation.

A. Hardware Components

The experimental setup used in this paper is shown in Fig. 6. The aluminium support frame is constructed in such a way that an LED can be moved freely on the x- and y axis. As a LS, the LED LZC-03MD07 from LED Engin is chosen, because it offers high power output with approximately 10W per color red, green, blue and white. For our experiments here, we have chosen the red and blue channel – blue because of the high lumen efficiency and red because of the enhanced responsivity of the PD – to get the most impact. Another reason are the color filters of the chosen RGB LCD. In order to avoid unnecessary signal loss, as each color only occupies one third of the pixel size, the LED colors are matched to the colors of the filters.

100 cm below the LED, the LCD is placed at a fixed position. In this paper, we use a commercially available Sharp LS055R1SX04 RGB LCD with removed backlight. Commonly,

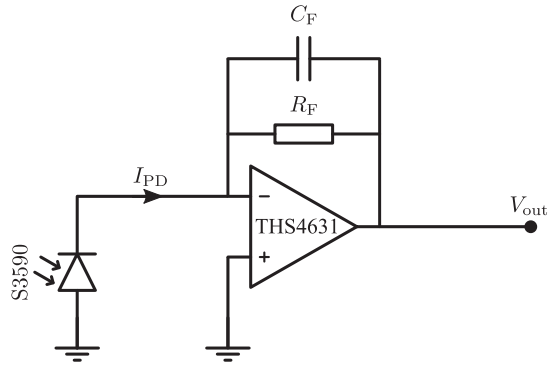

Fig. 7. Transimpedance amplifier in photovoltaic mode.

this kind of display is employed in 3D resin printers or in smartphones. It features a resolution of $n_x \times n_y = 2560 \times 1440$ pixels and thus belongs to the wide quad high definition (WQHD) category. The display is specified with a length of $l = 12.096$ cm and a width of $w = 6.804$ cm, resulting in a diagonal size of 5.5 in. Therefore, with (1) the edge length of one quadratic pixel can be calculated as $d_{\text{px}} = 4.725 \cdot 10^{-3}$ cm. The display features a refresh rate of $f_{\text{LCD}} = 60$ Hz.

As can be seen in Fig. 6, the LCD is connected via a HDMI cable to a computer which controls the display. A USB connection provides the power supply.

To guarantee a stationary position and height between PD and LCD, a dedicated, 3D-printed aperture is employed. At the top, a recess is provided for the LCD, which is designed such that the whole active area A_{LCD} can be viewed by the PD. The PD is placed below the LCD exactly at the center of the display at a fixed distance of $h = 5.5$ cm.

To capture as much light as possible, the large-area Hamamatsu S3590-08 Si PIN photodiode is chosen as PD. The S3590-08 has a photosensitive area of $A_{\text{PD}} = a^2 = 1\,\text{cm}^2$ and a high quantum efficiency. However, despite the large photosensitive area, the resulting photo current I_{PD} is still very small. In order to amplify the desired signal and to convert the current into a voltage [19]

$$V_{\text{out}} = -I_{\text{PD}} \cdot R_{\text{F}} \tag{25}$$

suitable for subsequent processing, the PD is placed on a board with a transimpedance amplifier (TIA) circuit (Fig. 7). The TIA consists of a feedback resistor R_{F}, an optional feedback capacitor C_{F} mitigating oscillations, and an operational amplifier (OpAmp). Operating the photodiode with a reverse bias voltage (called photoconductive mode) results in a faster response, while operating with zero bias voltage (known as photovoltaic mode) reduces the dark current. Since low-rate measurements and noise immunity are targeted, the photovoltaic mode is preferable. The Texas Instruments THS4631 is chosen as a high gain-bandwidth low-noise OpAmp. In the experimental setup $R_{\text{F}} = 500\ \text{k}\Omega$ is chosen, because the attenuation of the LCD in pass mode is relatively high.

The output of the OpAmp is connected to an analog-to-digital converter (ADC) which is integrated on an Arduino Portenta H7 microcontroller (μC). The ADC has an accuracy of 16 bit and

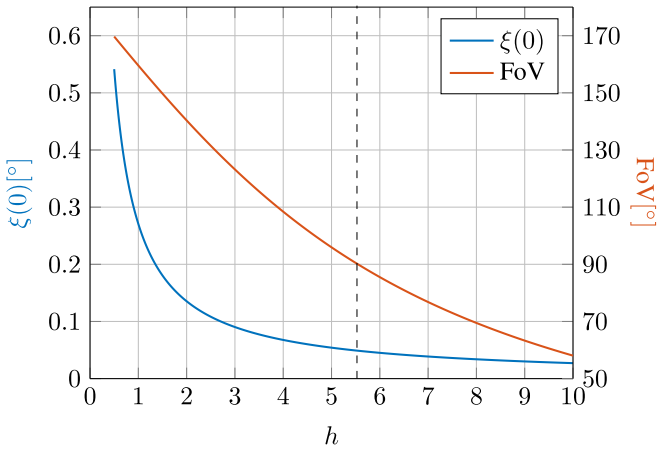

Fig. 8. Azimuth FoV and the angular resolution $\xi(0)$ at boresight with $\kappa = 1$ as a function of the height h between LCD and PD. The dashed line represents the chosen height h for the experimental setup.

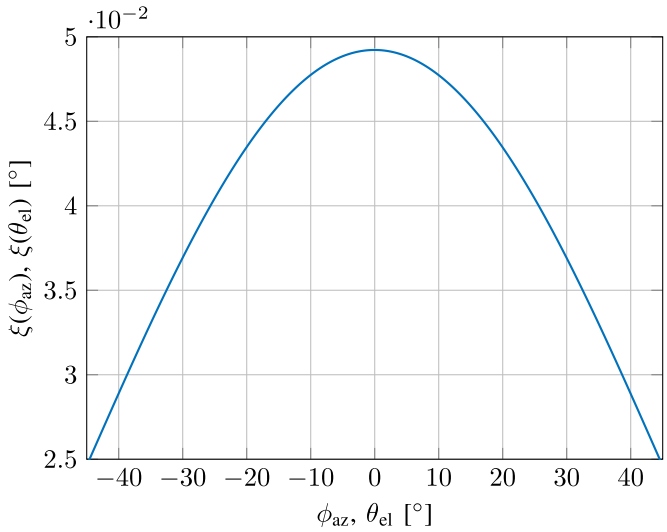

Fig. 9. Angular resolution $\xi(\phi_{\text{az}})$, $\xi(\theta_{\text{el}})$ as a function of the AoA ϕ_{az}, θ_{el} for $d_{\text{px}} = 4.725 \cdot 10^{-3}$ cm, $\kappa = 1$, $h = 5.5$ cm.

operates at a sample rate of 1 Msps. Communication between μC and computer is established via a serial interface.

B. Influence of the Experimental Setup on the AoA Estimation

The experimental setup presented in this paper has several adjustable parameters that affect the AoA estimation performance. Let us first of all analyze the trade-off between the FoV and the angular resolution ξ exemplary for azimuth angles. Again, the adaptation to elevation angles is straightforward. In the previous section, $l = 12.096$ cm, $d_{\text{px}} = 4.725 \cdot 10^{-3}$ cm, $a = 1$ cm and $h = 5.5$ cm were specified. Thus, with (2) and (3) a field-of-view of $\text{FoV}_{\text{az}} \approx 90.5°$ and $\text{FoV}_{\text{el}} \approx 55.6°$ is achieved for the experimental setup. For the analysis of the trade-off, we consider the angular resolution at boresight, i.e. $\xi(0)$. The resulting simplified equation (11) yields $\xi(0) \approx 0.05°$ for $\kappa = 1$. As mentioned in Section III-A, on the one hand the FoV decreases with increasing height h, on the other hand the angular resolution $\xi(0)$ improves with increasing height h. To illustrate this trade-off, in Fig. 8 both the FoV as well as $\xi(0)$ are depicted as a function of the height h. The dashed line represents the chosen height in the experimental setup. As can be seen from the course of the blue curve, $h < 3$ cm is not practical, because the change of $\xi(0)$, i.e. its slope, is greater for increasing h than the change of the FoV. Similarly, $h > 6$ cm is not practical, because the gain in angular resolution is only marginal. In the experimental setup $h = 5.5$ cm was chosen to achieve a good angular resolution with a sufficient FoV.

In the previous analysis, the angular resolution was considered at boresight, i.e. $\xi(0)$. However, as can be seen in (10), the angular resolution is AoA dependent. Inserting the calculated pixel edge length d_{px}, the specified height h and $\kappa = 1$ into (10), the AoA dependent angular resolution is obtained. Fig. 9 displays $\xi(\phi_{\text{az}})$, $\xi(\theta_{\text{el}})$ for an angular range from $-45°$ to $45°$. As expected from Section III-A, the worst case is at $0°$ and can be calculated according to (11) as $\xi(0) \approx 0.05°$. For $\kappa = 10$, the angular resolution is also reduced by a factor of 10 to $\xi(0) \approx 0.5°$. As can be seen in Fig. 9, the angular resolution improves with increasing AoA. The reason was explained in Section III-B: d_{px} is effectively reduced with increasing AoA. Thus, the LCD-based AoA estimator has the smallest accuracy for a target at boresight.

As mentioned in Section III-A and III-C, the LCD consists of an integer number of pixels. This makes it a challenge to generate a transparent area A_{tran} with the exact same width a as the photosensitive area A_{PD}. Therefore, n_{tran} must be rounded according to (5). Using the values from the experimental setup, i.e. $d_{\text{px}} = 4.725 \cdot 10^{-3}$ cm and $a = 1$ cm the true number of pixels is calculated as $n_{\text{tran}} = \sqrt{N_{\text{tran}}} \approx 211.64$. To allow an absolutely centered alignment of A_{tran} over the PD, n_{tran} is rounded to the next even integer, i.e. $n_{\text{tran}} = 210$ pixels. With this number of pixels a width $a \approx 0.9923$ cm is achieved. Such a small deviation should have a vanishingly small impact on the measurement results. This will be verified in Section V.

Finally, another influence on the AoA estimation performance is given by the refresh rate f_{LCD}, the resolution κ and the employed search algorithm. With the parameters specified in Section IV-A, the runtime of the exhaustive search algorithm can be calculated using (12). For $\kappa = 1$ a full search requires more than 17 hours to complete, which is exorbitantly high - just as indicated in Section III-B. There are four solution approaches conceivable. The first is the artificial reduction of the resolution with e.g. $\kappa = 10$. However, a full search would take more than 10 minutes - still unacceptable. To achieve a practical runtime, the resolution would have to be reduced significantly further at the expense of accuracy. The second solution approach is to employ an LCD with a higher frame rate. Unfortunately, this cannot reduce the runtime enough, since commercially available LCDs typically feature a refresh rate of up to 120 Hz. Even the high refresh rate of up to 360 Hz of specialized devices currently entering the market is worthy of improvement for the targeted measurement application. The third approach is to change the search strategy to the bar algorithm, which was introduced in Section III-B. The maximum runtime can be calculated with

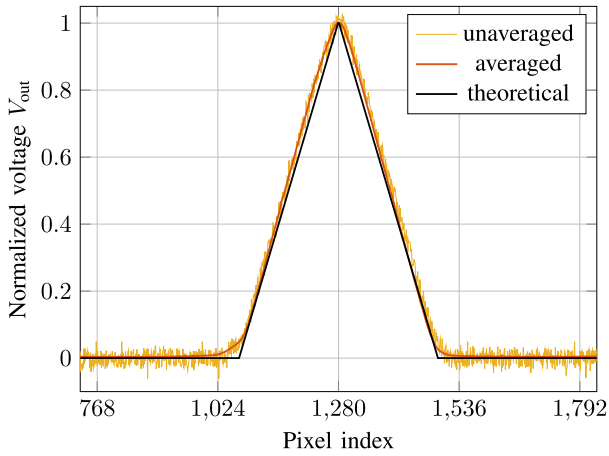

Fig. 10. Comparison of the theoretical prediction (black curve) with experimental results using a transparent square area with $\kappa = 1$. For the orange curve, each measurement value is averaged over 1000 samples. For the yellow curve, no averaging is done.

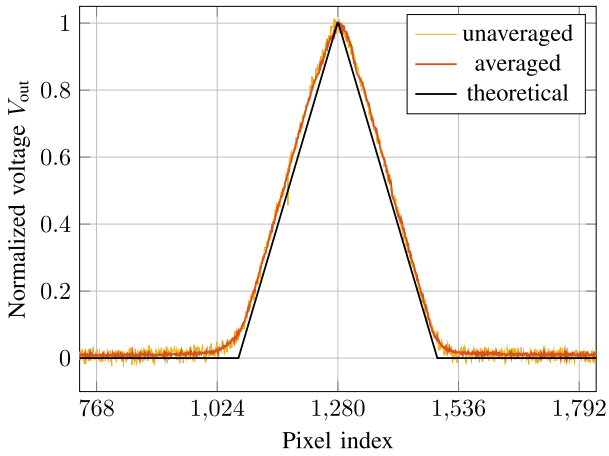

Fig. 11. Comparison of the theoretical prediction (black curve) with experimental results using the bar algorithm with $\kappa = 1$. For the orange curve, each measurement value is averaged over 1000 samples. For the yellow curve, no averaging is done.

(13). For $\kappa = 1$ the algorithm requires little more than 1 minute to complete. The artificial reduction with $\kappa = 10$ reduces the runtime to about 6.7 seconds. Finally, the bar algorithm can be combined with hill-climbing, which halves the expected rumtime.

C. Procedure of the AoA Estimation

To perform an LCD-based AoA estimation, a Matlab program is executed on the PC which creates a full screen plot on the connected LCD. Then, as described in Section III-B, a transparent bar is generated at $x = -\frac{l}{2}$ and moved in iterative steps along the discrete (virtual) pixel grid. Before each step, Matlab transmits a command over the serial interface to the μC to start the ADC sampling process and waits for an answer. Depending on the command, either 1, 10, 100, 1000 samples are recorded and averaged by the arithmetic mean to reduce measurement noise. Due to the high sampling rate of the ADC, this has almost no effect on the algorithm runtime. Afterwards, the result is transmitted back to the PC over the serial connection and stored in an array. This procedure is repeated until the right edge $x = \frac{l}{2}$ is reached and the number of averaged samples is equal to the number of (virtual) pixels in x-direction. After that, the same procedure is carried out for the y-direction. In the last step, Matlab analyzes the measurement vectors, finds the maximum values and determines the associated angles ϕ_{az} and θ_{el}.

V. Experimental Verification

All subsequent measurements described in this section are carried out for the experimental setup shown in Fig. 6. To reduce interference from other light sources, the construction is placed in a darkened room. Furthermore, for subsequent measurement results, 1000 samples are recorded and averaged in order to illustrate the compliance with the theory. For an accurate estimation, less samples are sufficient.

In a first measurement setup, we verify the analogy between the mathematical convolution and the signal measured with the introduced LCD-based AoA estimator. To this end, the LED is positioned at the origin of the coordinate system exactly perpendicular above the LCD. For the first measurement, a square transparent area with a width of 210 pixels is moved along the x-axis, as described in Section III-C in detail. The analysis is restricted to azimuth angles and $\kappa = 1$ is set. An adaptation to elevation angles is straightforward. The result is shown in Fig. 10 by the orange curve. For a good comparability, the DC-offset of about 0.1 V is removed from the measurement and the voltage is normalized to 1. Furthermore, to reduce measurement noise, one measurement value is composed of 1000 averaged samples. For comparison, the yellow curve shows the measurement signal without averaging. It it evident that the accuracy of the estimation will suffer if unaveraged data is used, since the algorithm always chooses the maximum value. As can be seen in Fig. 10, the averaged measurement result and the theoretical prediction (black curve) are nearly identical, which confirms the statement made in Section III-C that the LCD-based AoA estimation replicates the convolution operation. One reason why the measurement is somewhat wider around the maximum could be that the widths of A_{tran} and A_{PD} are not absolutely identical. Another deviation is that the measurement signal has a smoother transition between zero and the triangular shape. One possible cause is reflections of the light at the LCD aperture. This allows the light to reach the detector before A_{tran} overlaps the PD. A solution is to cover the interior of the aperture with a coating featuring a low reflectance, e.g. Vantablack. Another possible cause is that for the theoretical result in Section III-C a far-field scenario is assumed. For the experimental setup, the distance between LED and LCD is indeed much greater than h, however, the far-field assumption can only be applied as an approximation. In this case, the light impinging on the LCD is not necessarily a planar wavefront, allowing photons to reach the detector before A_{tran} overlaps the PD.

The second measurement is conducted for the bar algorithm with a bar width of 210 pixels. Results are shown in Fig. 11 for the azimuth direction. The orange curve is obtained for 1000

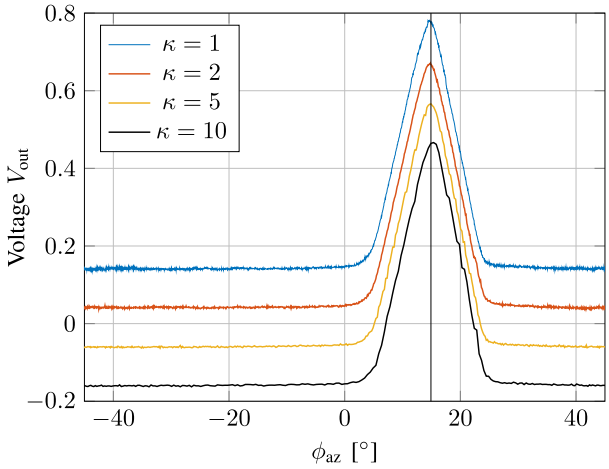

Fig. 12. Azimuth angle measurement results with different resolutions κ for an LED light source positioned at $\phi_{\text{az}} = 15°$, $\theta_{\text{el}} = -15°$. For all curves, each measurement value is averaged over 1000 samples.

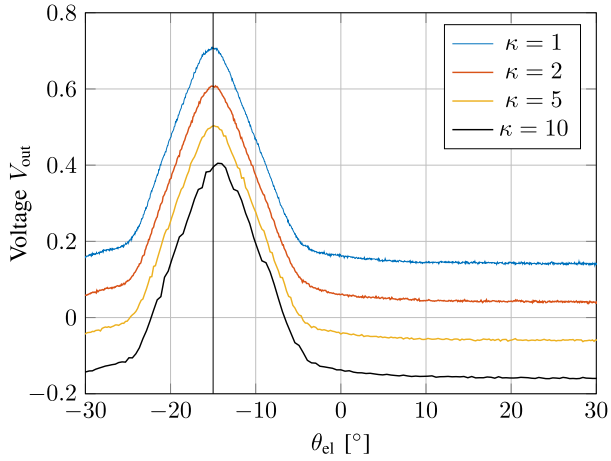

Fig. 13. Elevation angle measurement results with different resolutions κ for an LED light source positioned at $\phi_{\text{az}} = 15°$, $\theta_{\text{el}} = -15°$. For all curves, each measurement value is averaged over 1000 samples.

averaged samples. The yellow curve depicts the measurement signal without averaging. Again, the measurement result and the theoretical prediction (black curve) are nearly identical. This again confirms the statement made in Section III-C.

In the third measurement setup, the general AoA estimation capability is verified by positioning the LED LS at $\phi_{\text{az}} = 15°$, $\theta_{\text{el}} = -15°$ and performing a measurement with the bar algorithm. The results are depicted in Figs. 12 and 13 for different resolutions κ. The blue curve represents the measurement result with $\kappa = 1$, i.e. hardware pixel steps. For this measurement, the true voltage V_{out} can be read from the y-axis. For conciseness, the other three measurement results have been shifted down by 0.1 V each. The reason why the triangle shape of the elevation measurement is perceived wider is because the FoV is larger in azimuth direction. Restricting the angular range in the azimuth plot to the same as in the elevation plot would result in triangular shapes of identical width. Comparing the different resolutions, first of all it is observed that the general shape of the measurements is very similar. However, as expected, the accuracy is reduced for an increased κ. The black vertical line in both plots marks the true position of the LED. As can be seen, the measurements with $\kappa = 1$, $\kappa = 2$ and $\kappa = 5$ show good results whereas for $\kappa = 10$ the deviation of approximately $0.5°$ is significant. Still, as analyzed in Section IV-B, the worst angular resolution for $\kappa = 10$ is given as $\xi(0) \approx 0.5°$. Therefore, the measurement result is within the tolerance range.

In the final measurement setup, the LED LS is moved along the x-axis, i.e. in azimuth direction, from $-15°$ to $15°$ in $1°$ steps. The AoA estimation is performed with the bar algorithm at a resolution of $\kappa = 10$. At each angular step, five measurements are taken. The results ϕ'_{az} are shown in Fig. 14 by the blue circles. The reason why a maximum of three circles can be observed per angular step is that some of the estimation results overlap. More precisely, some results are identical, because the LCD-based AoA estimator can measure angles only at discrete intervals. Additionally, two black lines are integrated into the plot that show the true AoA with the angle-dependent angular resolution

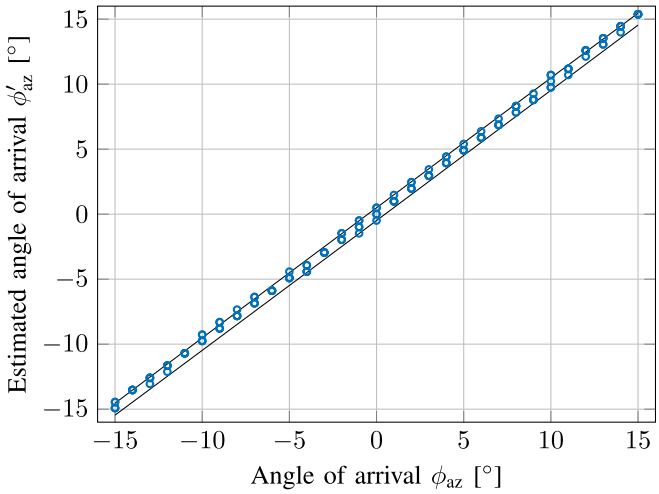

Fig. 14. Comparison between the true azimuth AoA ϕ_{az} and the estimated azimuth AoA ϕ'_{az} (circles). The two black lines show the true AoA, with the angle-dependent angular resolution added and subtracted, respectively.

$\xi(\phi_{\text{az}})$ for $\kappa = 10$ added and subtracted, respectively. The reason why the lines appear to be straight and parallel can be found when inspecting Fig. 9. Here, $\xi(\phi_{\text{az}})$ is plotted for $\kappa = 1$, however, for $\kappa = 10$ the shape is unchanged. Merely the y-axis values are increased by a factor of 10. Comparing the value at $0°$ with the values at $\pm 15°$ one finds that the difference is only marginal. Hence, in Fig. 14 no difference will be noticeable with the bare eye. Analyzing the estimation results ϕ'_{az}, it can be observed that, with a few exceptions, the estimated values lie exactly within the range given by $\xi(\phi_{\text{az}})$. Accordingly, a precise estimation of the AoA is possible with the LCD-based setup. The few estimations, which are slightly out of the given range, can be attributed to a misalignment of the LED as the LS is relocated manually.

VI. Conclusion

In this paper, a novel VLP technique is introduced, which employs an LCD as a dynamic receiver-side optical filter. With

this setup, light intensity can be measured from specific directions. Once the maximum light intensity is found, the AoA can be calculated from the known position of the transparent area.

In the description of the geometric scenario, it is discovered that the size of the transparent area plays a key role in the estimation process. Exclusively in the case where the A_{tran} is equal to A_{PD}, the estimation is without ambiguity. Furthermore, it is found that the angular resolution of the LCD is AoA dependent. Subsequently, it is revealed that the LCD setup creates a trade-off between the FoV and the angular resolution. Afterwards, two AoA estimation algorithms are found: the exhaustive search algorithm, which has an extremely high runtime and the so-called bar algorithm, which is faster but equally accurate. Then, a mathematical analogy for the LCD-based AoA estimation is pointed out. Interestingly, the process exactly replicates the convolution of two rectangular functions. Subsequently, the hardware components of an experimental setup are described. In this context, the trade-off between FoV and angular resolution is confirmed. Then, the AoA dependent angular resolution is investigated. It is confirmed that the LCD setup has the worst resolution at boresight, which improves with increasing AoA. Furthermore, it is recognized that the rounding error due to an integer number of pixels has a vanishingly small impact on the estimation. Finally, the above mentioned findings are verified by measurements conducted with the experimental setup. In a first step, the analogy between the LCD-based AoA estimation and the convolution operation is verified for both algorithms. In the next step, the general AoA estimation capability is verified by performing measurements with the bar algorithm for a LS placed at $\phi_{\text{az}} = 15^\circ, \theta_{\text{el}} = -15^\circ$. In the last step, a measurement is performed where the LS is moved along the x-axis from -15° to 15° in 1° steps. It is seen that, with a few exceptions, the estimated AoA values lie within the range determined by the angular resolution.

All in all, a very precise AoA estimation is possible with the introduced LCD-based technique. However, even with the bar algorithm the runtime is in the range of several seconds if a high-resolution LCD is taken. Therefore, for future work, it is interesting to investigate additional algorithms to reduce the search time. Furthermore, scenarios with multiple light sources should be considered and it should be investigated under which circumstances multiple sources can be reliably separated to determine their respective AoA.

REFERENCES

[1] J. Armstrong, Y. A. Sekercioglu, and A. Neild, "Visible light positioning: A roadmap for international standardization," *IEEE Commun. Mag.*, vol. 51, no. 12, pp. 68–73, Dec. 2013.

[2] N. Ul Hassan, A. Naeem, M. A. Pasha, T. Jadoon, and C. Yuen, "Indoor positioning using visible LED lights: A survey," *ACM Comput. Surv.*, vol. 48, no. 2, pp. 1–32, Nov. 2015.

[3] C. Gong, "Visible light communication and positioning: Present and future," *Electronics*, vol. 8, no. 7, Jun. 2019, Art. no. 788.

[4] P. A. Hoeher, *Visible Light Communications: Theoretical and Practical Foundations*. Munich, Germany: Carl Hanser, 2019.

[5] S. Arnon (Ed.), *Visible Light Communication*. Cambridge, U.K.: Cambridge Univ. Press, 2015.

[6] Y. U. Lee and M. Kavehrad, "Two hybrid positioning system design techniques with lighting LEDs and ad-hoc wireless network," *IEEE Trans. Consum. Electron.*, vol. 58, no. 4, pp. 1176–1184, Nov. 2012.

[7] W. Zhang and M. Kavehrad, "Comparison of VLC-based indoor positioning techniques," *Broadband Access Commun. Technol. VII*, vol. 8645, pp. 152–157, Feb. 2013.

[8] J. Vongkulbhisal, B. Chantaramolee, Y. Zhao, and W. Mohammed, "A fingerprinting-based indoor localization system using intensity modulation of light emitting diodes," *Microw. Opt. Technol. Lett.*, vol. 54, pp. 1218–1227, May 2012.

[9] B. Xie *et al.*, "LIPS: A light intensity-based positioning system for indoor environments," *ACM Trans. Sen. Netw.*, vol. 12, no. 4, pp. 1–27, Sep. 2016.

[10] T.-H. Do and M. Yoo, "TDOA-based indoor positioning using visible light," *Photonic Netw. Commun.*, vol. 27, no. 2, pp. 80–88, Apr. 2014.

[11] S.-H. Yang, H.-S. Kim, Y.-H. Son, and S.-K. Han, "Three-dimensional visible light indoor localization using AOA and RSS with multiple optical receivers," *IEEE/OSA J. Lightw. Technol.*, vol. 32, no. 14, pp. 2480–2485, Jul. 2014.

[12] S. Cincotta, A. Neild, C. He, and J. Armstrong, "Visible light positioning using an aperture and a quadrant photodiode," in *Proc. IEEE Globecom Workshops*, 2017, pp. 1–6.

[13] G. Wetzstein, D. Lanman, M. Hirsch, and R. Raskar, "Tensor displays: Compressive light field synthesis using multilayer displays with directional backlighting," *ACM Trans. Graph.*, vol. 31, no. 4, pp. 1–11, Jul. 2012.

[14] G. J. M. Forkel, A. Krohn, and P. A. Hoeher, "Optical interference suppression based on LCD-filtering," *Appl. Sci.*, vol. 9, no. 15, Aug. 2019, Art. no. 3134.

[15] A. Krohn, G. J. M. Forkel, P. A. Hoeher, and S. Pachnicke, "LCD-based optical filtering suitable for non-imaging channel decorrelation in VLC applications," *IEEE/OSA J. Lightw. Technol.*, vol. 37, no. 23, pp. 5892–5898, Dec. 2019.

[16] A. Krohn, S. Pachnicke, and P. A. Hoeher, "Genetic optimization of liquid crystal matrix based interference suppression for VLC MIMO transmissions," *IEEE Photon. J.*, vol. 14, no. 1, pp. 1–5, Feb. 2022.

[17] P. A. Hoeher, J. Sticklus, and A. Harlakin, "Underwater optical wireless communications in swarm robotics: A tutorial," *IEEE Commun. Surv. Tut.*, vol. 23, no. 4, pp. 2630–2659, Oct.–Dec. 2021.

[18] R. H. Chen, *Liquid Crystal Displays: Fundamental Physics and Technology*. Hoboken, NJ, USA: Wiley, 2011.

[19] P. Horowitz and W. Hill, *The Art of Electronics*, 3rd ed. Cambridge, U.K.: Cambridge Univ. Press, 2015.